JMB

Available online at www.sciencedirect.com

SCIENCE DIRECT®

ELSEVIER

Structural Mechanism Governing *Cis* and *Trans* Isomeric States and an Intramolecular Switch for *Cis*/*Trans* Isomerization of a Non-proline Peptide Bond Observed in Crystal Structures of Scorpion Toxins

Rong-Jin Guan[1]†, **Ye Xiang**[1]†, **Xiao-Lin He**[1], **Chun-Guang Wang**[1]
Miao Wang[1], **Ying Zhang**[1], **Eric J. Sundberg**[2] and **Da-Cheng Wang**[1]*

[1]*Center for Structural and Molecular Biology, Institute of Biophysics, Chinese Academy of Sciences, Beijing 100101 People's Republic of China*

[2]*Center for Advanced Research in Biotechnology, W.M. Keck Laboratory for Structural Biology, University of Maryland Biotechnology Institute, Rockville, MD 20850 USA*

*Corresponding author

Non-proline *cis* peptide bonds have been observed in numerous protein crystal structures even though the energetic barrier to this conformation is significant and no non-prolyl-*cis*/*trans*-isomerase has been identified to date. While some external factors, such as metal binding or co-factor interaction, have been identified that appear to induce *cis*/*trans* isomerization of non-proline peptide bonds, the intrinsic structural basis for their existence and the mechanism governing *cis*/*trans* isomerization in proteins remains poorly understood. Here, we report the crystal structure of a newly isolated neurotoxin, the scorpion α-like toxin *Buthus martensii* Karsch (BmK) M7, at 1.4 Å resolution. BmK M7 crystallizes as a dimer in which the identical non-proline peptide bond between residues 9 and 10 exists either in the *cis* conformation or as a mixture of *cis* and *trans* conformations in either monomer. We also determined the crystal structures of several mutants of BmK M1, a representative scorpion α-like toxin that contains an identical non-proline *cis* peptide bond as that observed in BmK M7, in which residues within or neighboring the *cis* peptide bond were altered. Substitution of an aspartic acid residue for lysine at residue 8 in the BmK M1 (K8D) mutant converted the *cis* form of the non-proline peptide bond 9–10 into the *trans* form, revealing an intramolecular switch for *cis*-to-*trans* isomerization. *Cis*/*trans* interconversion of the switch residue at position 8 appears to be sequence-dependent as the peptide bond between residues 9 and 10 retains its wild-type *cis* conformation in the BmK M1 (K8Q) mutant structure. The structural interconversion of the isomeric states of the BmK M1 non-proline *cis* peptide bond may relate to the conversion of the scorpion α-toxins subgroups.

© 2004 Elsevier Ltd. All rights reserved.

Keywords: cis/*trans* isomerization; non-proline peptide bond; structural mechanism; intramolecular switch; crystal structure

Introduction

The partial double-bond character of the peptide bond in proteins restricts its rotation such that consecutive C^α atoms exhibit coplanarity, and consequently, only *trans* and *cis* conformations are possible. The majority of peptide bonds adopt the *trans* conformation, as it is intrinsically favored energetically,[1,2] with the primary exception being peptide bonds formed between any amino acid and proline (Xaa–Pro), which have been observed in the *cis* configuration with greater frequency.[3] The observation of a *cis* peptide bond, especially of the non-proline *cis* variety, has been generally noted with great emphasis in the literature. Surveys of several databases[3–5] of protein structures, however,

---

† R.-J.G. & Y.X. contributed equally to this work.

Abbreviations used: Aah, *Androctomus australis* Hector; BmK, *Buthus martensii* Karsch; CT, C-terminal segment, residues 63–66; rBmK, recombinant BmK; RT, reverse turn residues, 8–12.

E-mail address of the corresponding author: dcwang@sun5.ibp.ac.cn

have revealed that the frequency of non-proline *cis* peptide bonds approaches one in every two thousand instances. Additionally, non-proline *cis* peptide bonds unequivocally identified in protein structures occur at or near functionally important sites more often than if their spatial distribution was random.[5,6] Renewed awareness of non-proline *cis* peptide bonds has led to a series of detailed analyses of their structural characteristics[5–7] and functional roles.[8–12] The structural mechanisms by which peptide bonds are converted from the energetically preferred *trans* conformation to that of the less favorable *cis* conformation, however, have received less attention.

Structural analyses of several proteins have shown that transformation of non-proline peptide bonds from *trans* to *cis* conformations can be induced by intermolecular binding events involving substrates, metals or co-factors that result in isomer-specific functional states.[8–11] The *cis–trans* isomerization of non-proline peptide bonds has also been observed in protein unfolding and refolding events in the absence of binding partners,[7,13–15] revealing that structural properties intrinsic to the protein can control the peptide bond conformations. The questions of how non-proline *cis* peptide bonds attain their energetically unfavorable conformation and which specific intramolecular structural elements are responsible for *cis* and *trans* conformations and their isomerization, however, have yet to be addressed rigorously. Here, we describe structural factors that govern the occurrences of *cis* and *trans* conformations of a non-proline peptide bond, as well as their co-existence, intrinsic to a class of scorpion neurotoxins. We also identify the intramolecular switch for *cis*-to-*trans* isomerization of this non-proline peptide bond.

Scorpion neurotoxins are known to interact specifically with voltage-dependent sodium channels.[16,17] Three phylogenetically distinct groups have been identified, classical α, α-like and α-insect toxins, which are highly toxic to mammals, insects and both insects and mammals, respectively.[18] The scorpion *Buthus martensii* Karsch (BmK) produces numerous neurotoxins, including BmK M1, M7 (both α-like) and M8 (classical α). The crystal structures of BmK M8[19] and M1[20] have revealed that the non-proline peptide bond between residues Pro9 and His10 exists in the *cis* conformation in BmK M1 but in the *trans* conformation in BmK M8, similar to other representative classical α toxins such as Aah2 (*Androctomus australis* Hector toxin 2).[21] This peptide bond is located within a five-residue reverse turn motif that contacts the C-terminal residue when it adopts the *cis* conformation in BmK M1, but makes no such intramolecular contacts when in the *trans* conformation in BmK M8.

Here, we describe crystal structures of BmK M7, which is unique in both its dimeric form and its extended C terminus, as well as of several mutants of BmK M1. In these structures, both the *cis* and *trans* conformations are observed for the non-proline peptide bond 9–10, as well as their co-existence

within a monomer in the asymmetric unit. We show that mutation at a site proximal to the non-proline *cis* peptide bond can act as an intramolecular switch for *cis*-to-*trans* isomerization. Furthermore, receptor specificity of these wild-type and variant scorpion toxins appears to be controlled by the backbone geometry of this particular non-proline peptide bond.

Results

Crystallographic sequencing of BmK M7

BmK M7 is an α-like toxin from the scorpion *Buthus martensii* Karsch (BmK), which resides in eastern Asia. It is comprised of 66 amino acid residues cross-linked by four disulfide bridges. Compared with most scorpion α-toxins containing 64 residues, which have only one residue after the terminal disulfide bridge Cys63–Cys12, BmK M7 is unique in having three C-terminal residues (Figure 1). The entire 66-residue sequence of BmK M7 was determined by crystallographic analysis and is shown in Figure 1. At 1.4 Å resolution, the electron density defining most residues is unambiguous. Loop residues 39–43, which exhibited poor electron density, were defined with the aid of homologous sequences from other BmK toxins (BmK M1, M2 and M4; Figure 1), as well as the experimentally determined molecular mass of 7237.4 from MALDI-TOF mass spectroscopic analysis. Glu/Gln and Asp/Asn residues were differentiated according to both the chemical environment as well as the homologous BmK toxin sequences.

Overall structure of BmK M7 dimer

The refined BmK M7 model contains two molecules in the asymmetric unit, related to one another by non-crystallographic 2-fold symmetry ($\sim 179.8°$), that form a homodimer through nine hydrogen bonds and numerous van der Waals contacts (Table 1). The structure of BmK M7 is the first scorpion toxin observed as a dimer. The protein regions associated with the non-proline *cis* peptide bond between residues Pro9 and His10, including the five residue reverse turn comprised of residues 8–12 and the neighboring C-terminal residues 63–66, are not involved in dimer formation. The dimer interface in BmK M7 displays a high degree of shape complementary, exhibiting a shape correlation coefficient (S_c) of 0.795 ($S_c = 1.0$ for interfaces with geometrically perfect fits),[22] and a large buried surface area of 911 $Å^2$, relative to the overall surface area of a 66-residue protein.

The two monomers in the BmK M7 dimer both adopt a general fold similar to the BmK M1, a representative BmK α-like scorpion toxin. All are composed of a dense core of secondary structural elements, including an α-helix formed by residues 19–28 and a three-stranded antiparallel β-sheet formed by residues 2–5, 32–37 and 45–51
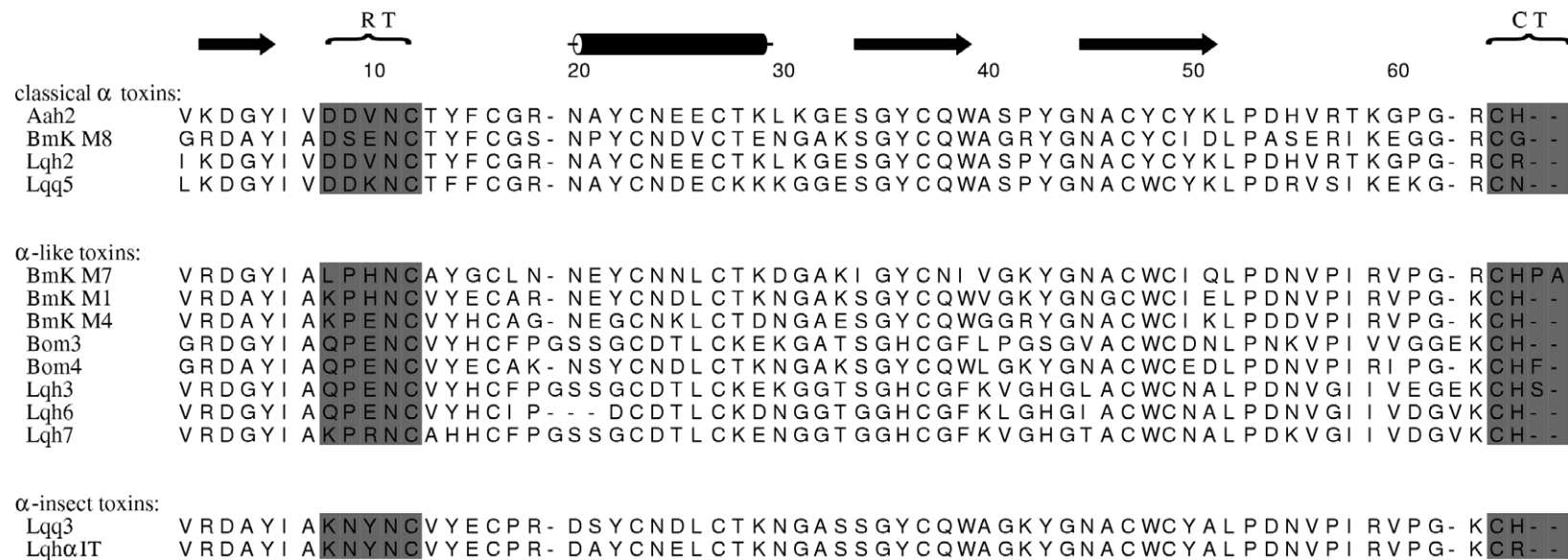
Figure 1. Sequence of BmK M7 and structure-based alignment of the amino acid sequences of different subgroups of scorpion alpha toxins. The positions are numbered in terms of BmK M1. Secondary structure elements are denoted on top of the sequences. The highly conserved cysteine residues are marked with dark in background. The residues of the unique site RT-CT formed by a five-residue reverse turn, in which a *cis* peptide bond occurs between residues 9 and 10, and the C-terminal segment are boxed. BmK M7 conspicuously has two additional residues at the C terminus. The sequences are from Possani *et al.*[39] and Hutchinson *et al.*[25] Sequence alignment was performed with CLUSTAL W[40] and the Figure was prepared with ALSCRIPT.[41]

Table 1. Interaction on the monomer–monomer interface in BmK M7

| Hydrogen bonds		
N19A O$^{\delta1}$	I38B O	3.12 Å
C36A O	I38B N	3.00 Å
N37A O$^{\delta1}$	N19B O$^{\delta1}$	2.87 Å
N37A O$^{\delta1}$	N37B O$^{\delta1}$	2.94 Å
N37A N$^{\delta2}$	N19B N$^{\delta2}$	3.12 Å
I38A N	C36B O	2.98 Å
N44A O$^{\delta1}$	N44B N$^{\delta2}$	2.75 Å
W47A N$^{\epsilon1}$	Y35B OH	3.03 Å

Hydrogen bonds were calculated using a cut-off of 2.5–3.5 Å.

(Figure 2). Three disulfide bridges (Cys16–Cys36, Cys22–Cys46 and Cys26–Cys48) stabilize this special βαββ motif. An additional disulfide bond between Cys12 and Cys63 cross-links a five-residue reverse turn (residues 8–12) with the C terminus to form a unique tertiary arrangement, hereinafter referred to as reverse turn-C terminus (RT-CT). Superposition of the two monomers (residues 9–10, 39–43 and 64–66 excluded) results in a root mean squared deviation (RMSD) of 0.448 Å for the main-chain atoms. There are three segments, however, including residues 9–10, 39–43 and 64–66, that exhibit distinct conformational states in the individual monomers. Residues 39–43, which form the B loop in other BmK α-like toxins, display extremely high flexibility in both BmK M7 monomers (Figure 2). Even at the final stage of refinement, the electron density could not be fit. In fact, in the structure of BmK M7, if seen from the crystal packing along *c* axis, this loop is located on the molecular surface and protrudes into a large hole formed by the crystal packing architecture. In previously determined scorpion α-toxin monomer structures,[19–21] this loop exhibits variant but definite conformations, constrained by crystal packing interactions. The flexible conformation of this loop that appears in the present BmK M7 dimer structure may more accurately reflect its conformational state in solution. Recently, site-directed mutagenesis analysis has implicated residues Trp38 and Tyr42 at this loop are involved in the pharmacological function of the toxin,[23] indicating that flexibility of this loop may play a role in toxin-receptor binding.

Non-proline *cis* peptide bond in molecule A of BmK M7

During refinement it was impossible to restrain the ω value of the peptide bond Pro9–His10 in molecule A near $\pm 180°$, whereas the ω angle went favorably towards 0°. Both $2F_o-F_c$ and F_o-F_c electron density maps (Figure 3(A) and (B)) definitively show that this peptide bond adopts a *cis* conformation in which the amide nitrogen is provided by an amino acid (His10) other than proline, classifying this as a non-proline *cis* peptide bond. Moreover, the C-terminal segment in BmK M7, which extends beyond other α-like toxins, exhibits an ordered conformation with clearly defined electron density (Figure 3(A)). Three main-chain hydrogen bonds between this segment and residues 9 and 10 were observed (Figure 5(A)). These local tertiary interactions likely play a crucial role in stabilization of the energetically unfavorable *cis* conformation of the peptide bond 9–10. An intermolecular contact between the main-chain O of the terminal residue Ala66 and the N$^{\zeta}$ atom of residue Arg58 from a symmetry-related molecule (Figures 2 and 5(A)), may provide energetic stabilization for the C terminus conformation.
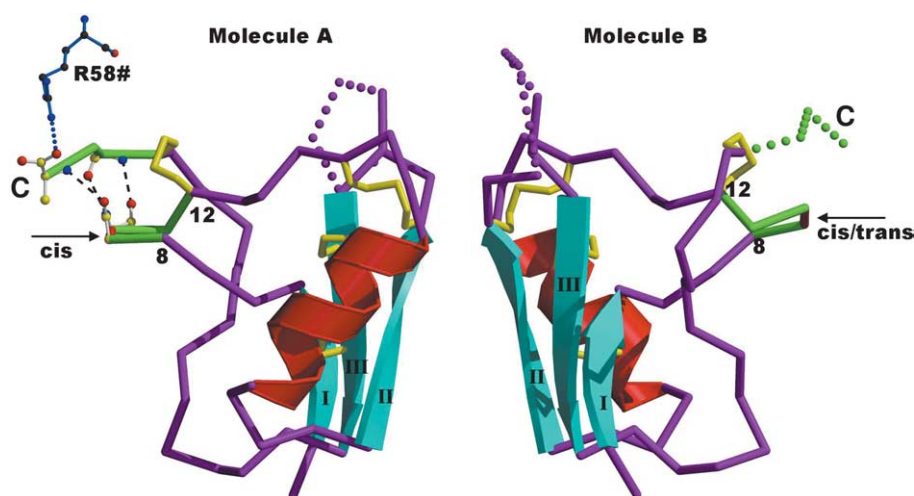
Figure 2. Ribbon diagram of the dimeric structure of BmK M7 in the asymmetric unit. The two monomers are related to each other by a 2-fold NCS axis. The five-residue reverse turn 8–12 and the C-terminal segment 63–66 are highlighted in green. The Pro9–His10 peptide bond in the reverse turn is indicated by arrow, which adopts *cis* form in molecule A and *cis/trans* co-existence in molecule B. Three hydrogen bonds between the 9–10 *cis* peptide and the C-terminal stretch, in addition to an intermolecular interaction between O66 and the asymmetric N$^{\epsilon}$58 in molecule A are also shown. The broken line shows the flexible part in the model. The Figure was prepared with MOLSCRIPT[42] and rendered by Raster3D.[43]
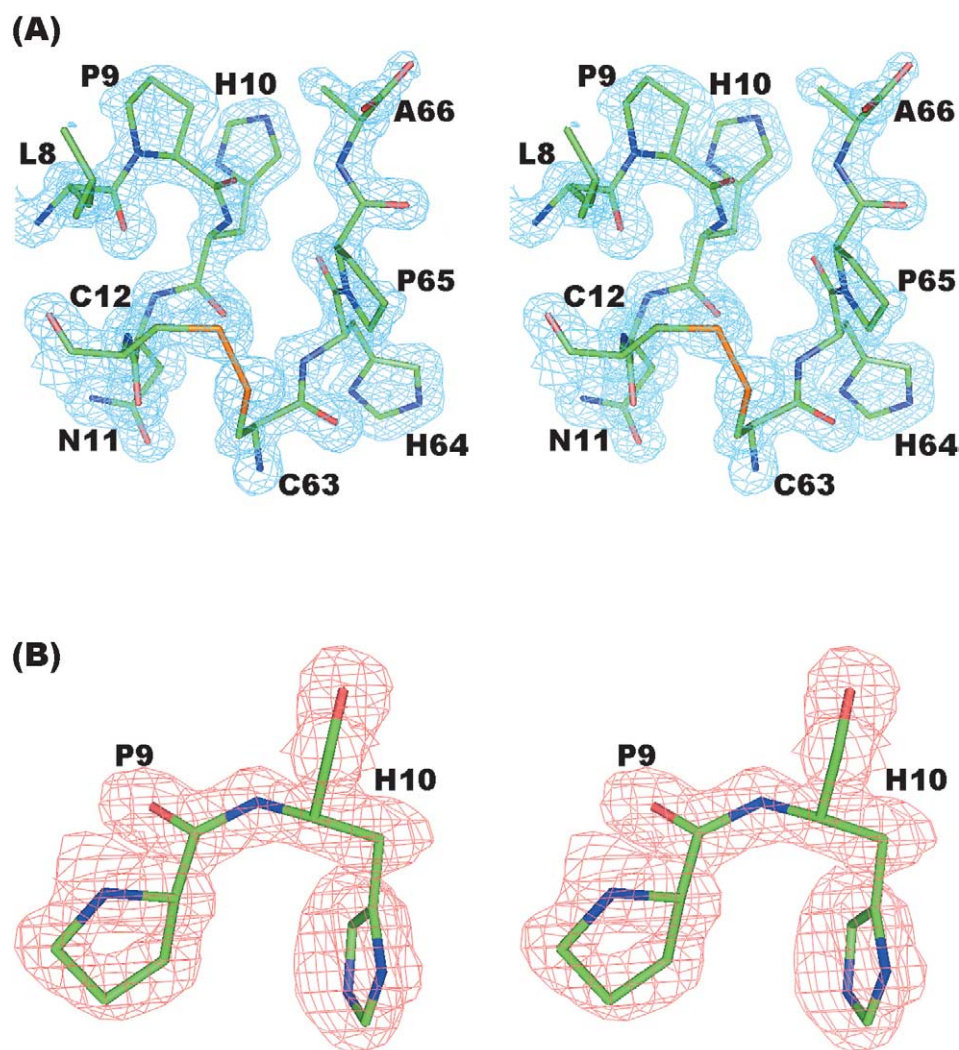
Figure 3. Electron density maps for the site RT-CT in molecule A of BmK M7. (A) σ_A-Weighted $2F_o - F_c$ maps around the five-residue reverse turn (8–12) and the C-terminal segment (63–66) (contoured at 1.5σ). All the residues can fit into the high-resolution densities very well, indicating definite conformation for this part in molecule A. (B) The omit $F_o - F_c$ electron density map around residues 9 and 10 (contoured at 3σ). In the calculation all atoms of residues 8–11 are omitted and here the only contours shown are those corresponding to the atoms of residues 9 and 10, which definitely show a *cis* configuration at the 9–10 peptide bond. The Figures were prepared with O.[37]

Co-existence of *cis* and *trans* isomers in molecule B of BmK M7

In the dimer structure of BmK M7, the peptide bond Pro9–His10 in molecule B exhibits a *cis/trans* dual-configuration (Figure 4), rather than the *cis* conformation observed in molecule A. Throughout the refinement, electron densities around the Pro9–His10 peptide bond in molecule B appeared relatively broad, and could not be fitted exclusively by either *cis* or *trans* conformations. During the earlier stages of the refinement, no special restriction was imposed on this peptide bond. After several cycles of model rebuilding and refinement, the quality of the model and the density maps were greatly improved (with R_{free} below 0.20). An unbiased difference ($F_o - F_c$) electron density map was calculated prior to inclusion of either *cis* or *trans* conformations for the peptide bond 9–10, which

showed a co-existence of the two conformations. In order to identify whether the *cis* and *trans* forms existed coincidentally at the peptide 9–10, two σ-weighted $F_o - F_c$ electron density maps were further calculated. The first calculation included the *cis* peptide bond prior to inclusion of the *trans* configuration, into which a *trans* conformation model can be built into positive electron density while a *cis* peptide bond fits well into the negative density (Figure 4(B)). Conversely, when an $F_o - F_c$ map is calculated using a model for the *trans* conformation, the *cis* peptide bond 9–10 can be built into the positive density, while a *trans* conformation can be built into negative density (Figure 4(C)).

The final $2F_o - F_c$ and $F_o - F_c$ electron density maps reveal that the C-terminal segment comprised of residues 64–66 is disordered (Figure 4(D)). All of the intramolecular contacts between the C-terminal residues and the peptide bond 9–10 observed in
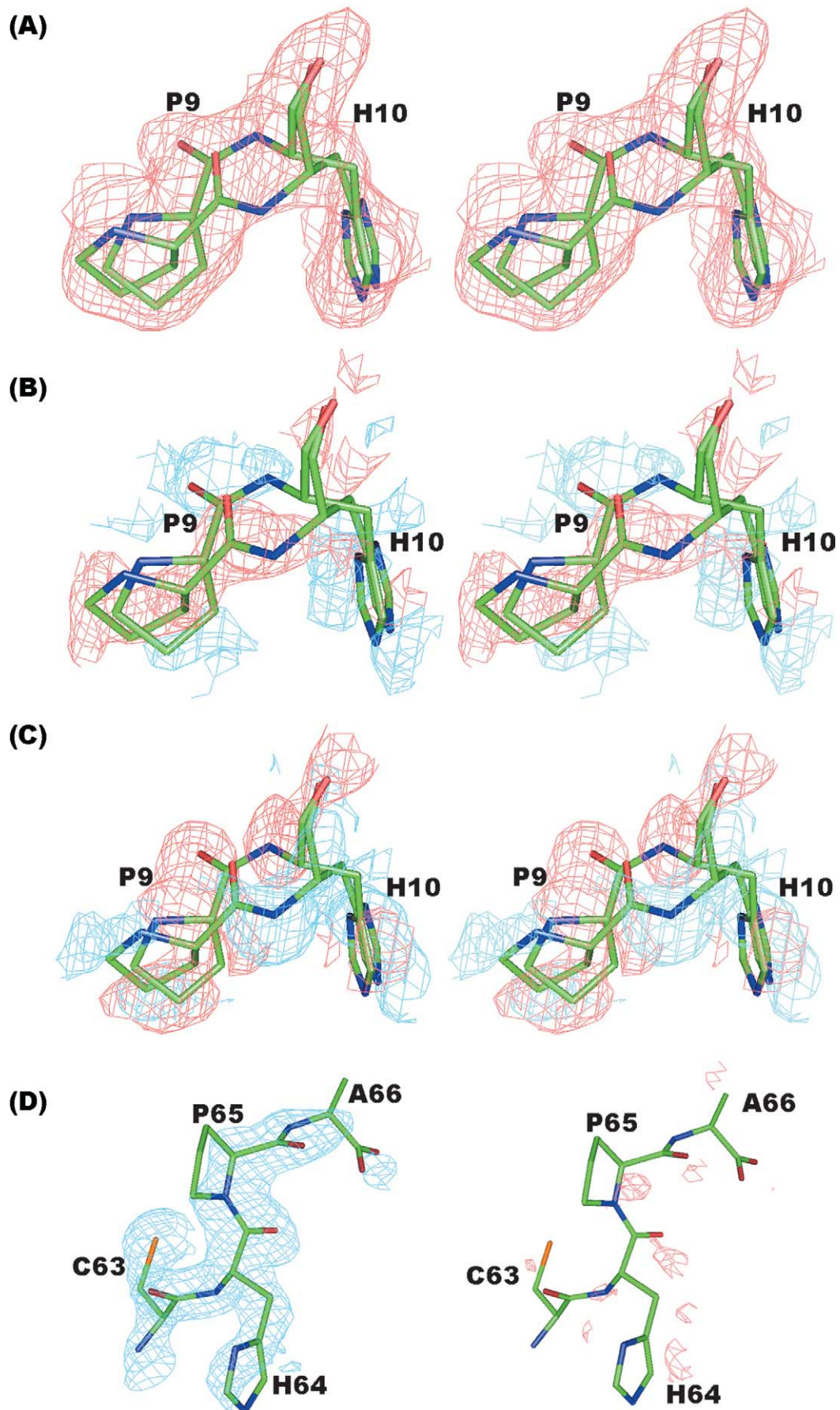
Figure 4. Electron densities around residues 9 and 10 and 63–66 in molecule B of BmK M7 showing the co-existence of

molecule A are absent in molecule B, providing a rationale for the structural basis for the existence of strict *cis* conformation of this peptide bond *versus* a mixed population.

In the final stage of refinement, the dual *cis* and *trans* conformations for residues Pro9 and His10 (with atomic occupancy 0.5) were built into the model of molecule B, resulting in decreases in both R_{cryt} and R_{free} from 0.1679 to 0.1669 and from 0.1864 to 0.1840, respectively. This implies that the inclusion of the dual conformation of the peptide 9–10 in molecule B is closer to the actual BmK M7 structure and co-existence of *cis* and *trans* conformations in the peptide bond 9–10 is objective.

Expression, purification and bioassay of BmK M1 mutants

To explore the key structural factors responsible for the *cis/trans* conversion of the peptide bond between positions 9 and 10, all residues in the vicinity of the *cis*-peptide bond are taken into consideration during the mutagenesis design, including residues 8, 9, 10 and 11. However, structural and sequence comparisons clearly show that the residue type of position 10 varies irregularly, which can be the same residue (Glu) in both *cis*- and *trans*-containing toxins, and also the different types in the same *cis*-containing toxins (His or Glu) or the same *trans*-containing toxins (Val or Glu or Lys). For residue Asn11, it is invariant in either *cis* or *trans* form toxins (Figure 1). Therefore, residues 10 and 11 should not be related to the *cis* or *trans* form of the peptide bond 9–10. At the same time residue 8 is conserved as Asp in all *trans* form toxins and residue 9 is conserved as Pro in all *cis* form toxins (Figure 1). Based on these analyses, residues 10 and 11 are set aside from the mutagenesis consideration and the emphasis is focused on residues 8 and 9.

Five mutants of BmK M1 were constructed, including mutations of the flanking Lys residue at position 8 with Asp (K8D), Asn (K8N), Glu (K8E) and Gln (K8Q), as well as replacement of Pro at position 9 with Ser (P9S). Of these, the K8N and K8E mutants did not express in our recombinant system. The molecular masses of the three other variants, K8D, K8Q and P9S, were measured by mass spectrometry and found to agree well with their respective theoretical values.

The LD$_{50}$ of wild-type BmK M1 determined by the method described by Meier & Theakston[24] was

Table 2. Expression and toxicity of the five BmK M1 mutants

Toxins	Expression (mg/l)	Toxicity (LD$_{50}$) (mg/kg)	Relative toxicity (%)
Wild-type rBmK M1	~5	0.53	100
K8D	10–11	>50	<1
K8N	None	–	–
K8E	None	–	–
K8Q	5–6	0.50	106
P9S	4–5	0.95	55

~0.53 mg/kg, which is consistent with that of native BmK M1.[30] Excluding K8N and K8E, which were not expressed, the other three mutants (K8D, K8Q and P9S) were used for bioassays. The toxicity of mutant K8D was lost in mice, while mutant K8Q was almost unchanged in comparison with unmodified rBmK M1 (Table 2). Mutant P9S exhibited the toxicity in the same order (55%).

Cis–trans conversion of the peptide bond 9–10 in the BmK M1 K8D mutant

The structure of mutant K8D at 1.5 Å resolution clearly revealed that the non-proline *cis* peptide bond between residues 9 and 10 in the native BmK M1 was converted to the *trans* conformation in the K8D mutant. Correspondingly, both $2F_o - F_c$ and $F_o - F_c$ electron density maps show the C$^\alpha$ atoms of residues 9 and 10 in K8D located on opposite sides of the 9–10 peptide bond. Accompanying the *cis–trans* conversion, both the N main-chain atom of His10 and the side-chain of Asp8 are rotated into the reverse turn relative to wild-type BmK M1. These changes force the five-residue reverse turn (residues 8–12) to adopt a new conformational state, in which the residues at positions 8 and 10 form an extensive hydrogen-bonding network (Figure 6), characteristic of the *trans* peptide bond-containing reverse turn in classical α scorpion toxins. The conformational transition of the peptide bond between residues 9 and 10 in the K8D mutant results in the abolition of contacts between the peptide bond 9–10 and C-terminal residues save a single hydrogen bond between main-chain atoms of residues His10 and His64 (Figure 6).

cis and *trans* configuration at the peptide bond 9–10 and the flexible C-terminal segment. (A) A completely unbiased $F_o - F_c$ map prior to inclusion of either *cis* or *trans* model. The spread densities showed a mixture of *cis* and *trans* configurations at the peptide 9–10. (B) $F_o - F_c$ map calculated with *cis* peptide 9–10 model but prior to inclusion of *trans* configuration. Against the map, a *trans* model can be built up in positive densities (in red) and a *cis* form can fit into negative densities (in blue). (C) $F_o - F_c$ map after inclusion of the *trans* peptide 9–10 but without *cis* configuration, in which the *cis* peptide 9–10 can be modeled in positive densities (in red) and a *trans* form can be built into negative densities (in blue). In the calculation of above maps the residues 8–11 are omitted and the only densities shown in height red (positive) and blue (negative) are those corresponding to the peptide 9–10. All $F_o - F_c$ maps are σ-weighted and contoured at 2σ or −2σ. (D) $2F_o - F_c$ map (contoured at 1σ) (left) and $F_o - F_c$ map (contoured at 2σ) around residues 63–66 in molecule B showing flexibility of the C-terminal segment 64–66 in molecule B. The drawings were prepared with PYMOL.[33]

Cis form of the peptide bond 9–10 in mutants K8Q and P9S

Contrary to the K8D mutant, replacement of residue Lys8 with Gln results in retention of the *cis* conformation of the peptide bond 9–10 found in wild-type BmK M1. Consequently, the intramolecular contacts between residues from the reverse turn and the C terminus are similar to those in wild-type Bmk M1 (Figure 6). The structure of mutant P9S also revealed a *cis* conformation for the peptide bond 9–10. Sequence alignment indicates that Pro9 is conserved in *cis*-containing toxins (Figure 1). The structure of the P9S mutant indicates that the Pro residue at position 9 is not required for the peptide bond 9–10 to adopt the *cis* conformation. Lack of expression of the K8E and K8N mutants may indicate the importance of residue 8 not only in governing the conformational state of the five-residue reverse turn in the folded molecule, but also in subsequent correct global folding of the toxin molecule.

Discussion

Structural properties of differential peptide bond 9–10 isomeric states

Surveys of structural databases[3–5] have revealed the occurrence and biological importance of non-proline *cis* peptide bonds in protein structures. Detailed analyses of the conformational characteristics and functional roles of these unusual peptide bonds have been reported.[8–12] External structural factors, such as substrate binding, metal binding, or co-factor interaction, have been identified as inducers of the *cis*/*trans* isomerization. How non-proline peptide bonds attain their distinct *cis*/*trans* isomeric states and which structural factors specifically govern the occurrence of different isomers, however, have yet to be addressed rigorously. The observations here reveal one way by which the specific intramolecular structural factors govern a non-proline peptide bond to attain *cis* or *trans* conformations, or *cis*/*trans* co-existence.

In the crystal structures of dimeric BmK M7 and three BmK M1 mutants (K8D, K8Q and P9S) three distinct isomeric states of the non-proline peptide bond 9–10 are observed, including *cis* (BmK M7 molecule A and BmK M1 mutants K8Q and P9S), *trans* (BmK M1 mutant K8D), and the co-existence of *cis* and *trans* (BmK M7 molecule B) conformations. Detailed inspection and comparison of these structures reveal that these isomeric states are dependent on the distinct tertiary arrangement of the five-residue reverse turn (residues 8–12) and the C-terminal segment (residues 63–66). In the *cis* conformation, both the main-chain O and N atoms of residues 9 and 10, respectively, extend away from the reverse turn and interact with the C-terminal residue 64 *via* a hydrogen bond between the main-chain N and O atoms of residues 10 and 64,

respectively. This results in a protrusion of the side-chain of residue 8 from the reverse turn. In the *trans* conformation, however, the main-chain N atom of residue 10 turns into the core of the reverse turn and, correspondingly, interacts with the side-chain of residue 8, giving rise to the extensive hydrogen-bonding network of the reverse-turn structure (Figure 6). This results in the abrogation of the interaction between the peptide bond 9–10 and C terminus. When *cis* and *trans* conformations co-exist within a single molecule, the main-chain N atom of residue 10 contacts neither a C-terminal residue nor the side-chain of residue 8 (Figure 5), resulting in a novel reverse turn structure that cannot be classified as one of the canonical β-turn defined by Hutchinson & Thornton.[25]

Regardless of the peptide bond 9–10 heterogeneity exhibited in these structures, the reverse turn motifs in all BmK toxins share a number of common structural features. The final two turn residues, Asn11 and Cys12, are strictly conserved (Figure 1) and form multiple contacts with the C-terminal segment in all scorpion α-toxin structures determined so far,[20] including a disulfide bond. The highly constrained reverse turn-C terminus (RT-CT) structural motif accounts for the tendency of the *cis* conformation, isomerization to the *trans* conformation and the co-existence of both isomers for the peptide bond 9–10 in BmK toxins. The structures reported here indicate that the *cis* conformation of the peptide bond 9–10 is energetically favorable to the structural organization of the RT-CT motif. In this case, the myriad interactions between the reverse turn in which the peptide bond 9–10 resides and the C-terminal segment appear capable of overcoming the normally energetically favored *trans* peptide bond conformation. Conversely, altered interactions within the core of the reverse turn arising from mutation of Lys at position 8 to Asp in BmK M1 invert the energetic parameters as to allow the K8D mutant to adopt the *trans* conformation.

The conformational state of the main-chain N atom of residue 10 is the structural signature of the distinct isomeric states of the peptide bond 9–10. When this atom protrudes into the reverse turn and interacts with the Asp side-chain in the K8D mutant, the peptide bond adopts the *trans* conformation. When it instead protrudes out of the reverse turn and interacts with the main-chain carbonyl of the C-terminal residue 64 it is found in the *cis* conformation (Figure 6). In the absence of intramolecular atomic interactions for the residue 10 N atom, the peptide bond 9–10 co-exists in both the *cis* and *trans* isomers (Figure 5(B)). Although additional interactions, such as between main-chain atoms of residues 9 and 10 with those from the C-terminal segment, are present in this region of the molecule and may play a role in stabilization of the local RT-CT structural motif, they appear insufficient to control the isomeric state of the peptide bond 9–10.

An intramolecular switch governs peptide bond isomerization

The molecular switch for *cis/trans* peptide bond isomerization at position 8 of BmK M1 is sequence-dependent. As described above, mutation of the wild-type Lys residue at this position to Asp (K8D) results in a *cis*-to-*trans* isomerization of the peptide bond, while mutation to Gln (K8Q) maintains the *cis* conformation of the wild-type protein. Our attempts to express BmK M1 mutants with similar amino acid changes at position 8, including Glu (K8E) and Asn (K8N), were unsuccessful (Table 2). This suggests the intriguing possibility that these mutants represent a third outcome of the molecular switch for peptide bond isomerization at position 8, which results in a local structure that is incompatible with the global folding of the protein. As the five-residue reverse turn in which this molecular switch resides is, respectively, conserved in different groups of scorpion α-toxin (Figure 1), its sequence-dependent nature may also extend to other members of this toxin family. Thus, it can be predicted that replacing residue 8 in other scorpion
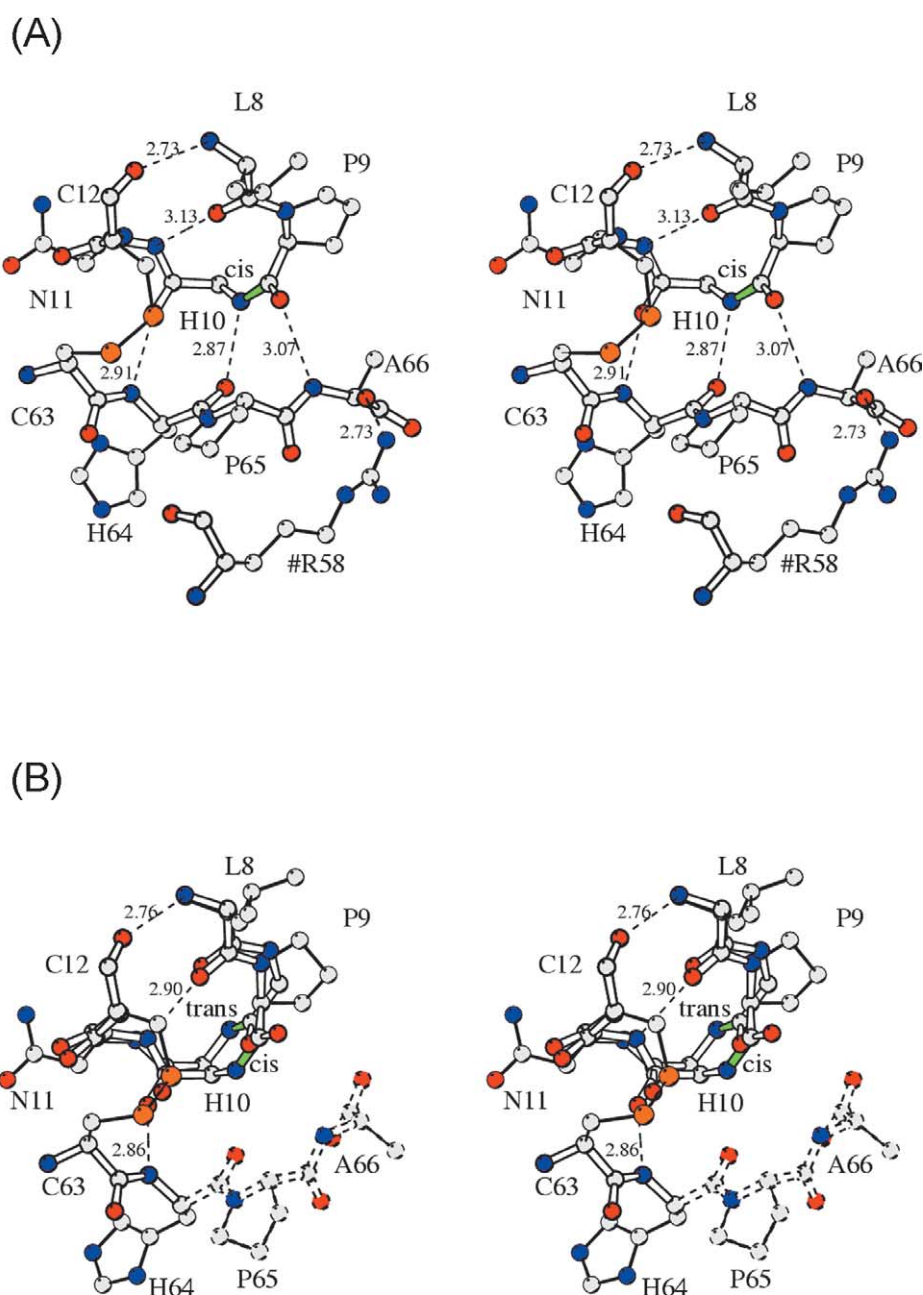
Figure 5. Structure of the five-residue reverse turn and C-terminal segment in M7-A (A) and M7-B (B). In M7-A the peptide bond 9–10 adopts *cis* form and both NH10 and CO9 groups of the peptide are out of the reverse turn to interact with the C-terminal residues. In M7-B the group NH10 contacts neither residue 8 nor C-terminal residues in flexible state and, thus, the peptide bond 9–10 takes *cis/trans* co-existence. For clarity the side-chains of residues 8–12 are only shown corresponding to the *cis* form of the peptide 9–10, with deletion of His10 not shown in the Figures.
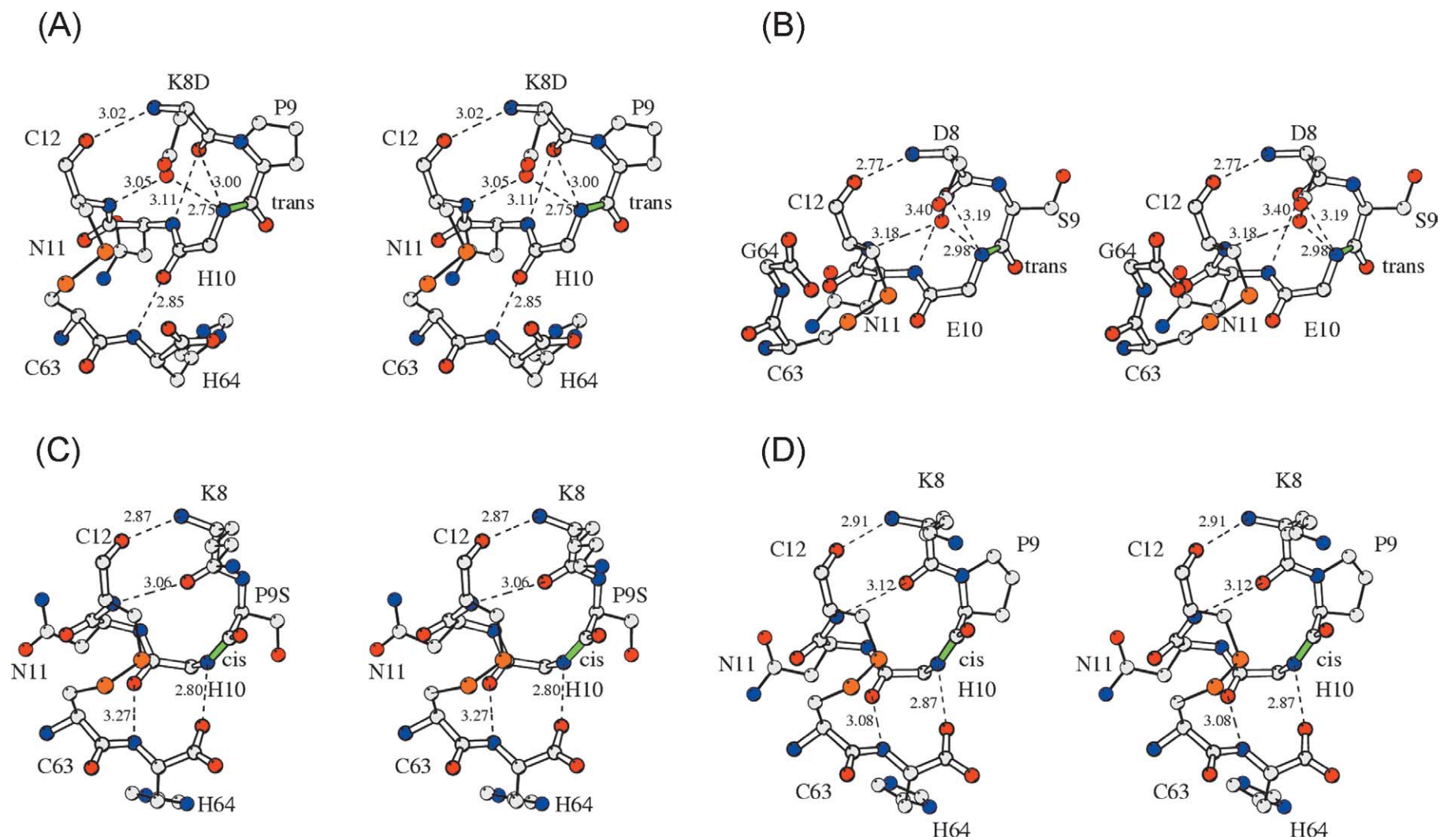
Figure 6. Distinct structures of the five-residue reverse turn and C-terminal residues of the *trans*-containing site RT-CT in BmK M1 K8D mutant (A) and native BmK M8 (B), and the *cis*-containing RT-CT in BmK M1 K8Q mutant (C) and native BmK M1 (D). In the *trans*-containing form (A) and (B), the peptide group NH10 is situated inside the turn and the residue 8 must be Asp; these two interact with each other *via* hydrogen bond N10…O$^{\delta1}$8, but there is no contact between the NH10 group and the C-terminal residue. In *cis*-containing form (C) and (D) group NH10 is out of the reverse turn and interacts with the C-terminal residue *via* hydrogen bond N10…O64. Meanwhile the residue 8 is non-aspartic and protrudes from the turn. In this case the reverse turn is well stabilized by two main-chain hydrogen bonds between residues 8 and 10. For clarity the side-chain of residue 10 is not shown in all Figures. The Figures were prepared with MOLSCRIPT.[42]

toxins with Asp, Lys/Gln, or Asn/Glu will result in a peptide bond 9–10 adopting a *trans*, *cis*, or misfolded protein, respectively. It is possible to experimentally validate this prediction.

Possible biological significance of variable RT-CT structural motif conformational states

Variable conformations of the peptide bond 9–10 result in three unique structural organizations of the RT-CT motif. In the first motif, termed *trans*RT-*far*CT and exemplified by BmK M8[19] and Aah2[21] (Figure 7(A)), the *trans* peptide bond 9–10 mediates an extensive hydrogen bonding network internal to the RT and a paucity of intramolecular interactions with the CT residue 64. The second motif, *cis*RT-*close*CT (Figure 7(B)), is characterized by the *cis*-containing RT structures of BmK M7 molecule A, BmK M1 and associated mutants K8Q and P9S, in which extension of the main-chain amine and carbonyl groups of the peptide bond 9–10 to the periphery of the RT facilitates intimate contact with the CT segment. The third motif, *trans*RT-*close*CT (Figure 7(C)), exhibited by the BmK M1 K8D mutant, is a fusion of an RT structure common to the *trans* peptide bond 9–10 and the interacting CT segment similar to toxins exhibiting *cis*-containing RT structures. The unique structures of the RT-CT motif are stabilized by the disulfide bridge Cys12–Cys63, which exhibits structural variability amongst different toxins, such as BmK M8,[19] M1[20] and Aah2.[21]

These three RT-CT conformational motifs provide a possible structural basis for the binding preference of three α-toxin subgroups for phylogenetically distinct, yet closely related, target sites on the sodium channel. The pathogenicity of scorpion α-toxins is caused by binding to the fourth domain of the α-subunit of the target sodium channel,[26] resulting in a prolonged action potential due to retardation of the inactivation event. Scorpion α-toxins can be classified into pharmacological subgroups according to their preferential toxicity to mammals or insect.[27] The evidence supports their binding to a homologous cluster of partially overlapping sites located on the sodium channel surfaces in both mammals and insects.[18,27] Recently, site-directed mutagenesis analysis of BmK M1, a representative α-like toxin, identified a functional site that includes residues Lys8, Asn11, Arg58, Lys62 and His64[28] and is generally coincident with the RT-CT structural motif described here.

The variable conformation of this functional site may have significant biological ramifications. The classical α-toxins BmK M8[19] and Aah2[21] take the *trans*RT-*far*CT motif (Figure 7(A)) and are highly toxic to mammals. Adoption of this structural motif renders the functional residue Arg58 inaccessible to ligand due to steric hindrance by the CT region.[19] The α-like toxins BmK M1, M2 and M4,[20] as well as M7 and its associated mutant K8Q (this work), adopt the *cis*RT-*close*CT motif (Figure 7(B)) and exhibit full toxicity to both mammals and insects.

The functional residue Arg58 in these structures is solvent-accessible and able to engage ligand.[20] Mutation of Lys8 to Asp functions not only as a molecular switch in isomerizing the peptide bond 9–10 from the *cis* to *trans* conformation and consequent adoption of the *trans*RT-*close*CT motif (Figure 7(C)), but also as a switch for biological function. The bioassay revealed that the toxic effects of this mutant have been lost in mice (Table 2), while electrophysiological characterization using the cloned Para/tipE insect sodium channel showed that the BmK M1 K8D mutant retained its functionality responsible for insect toxicity (J. Tytget, personal communication). Accordingly, the conformational state of the *trans*RT-*close*CT motif in α-like toxins may also be related to sodium channel binding site selectivity. These observations show one way in which high levels of molecular specificity and biological function may be achieved primarily through *cis/trans* isomerization of a critical peptide bond.

Comparison of the conversion mechanism for *cis/trans* isomerization of BmK toxins with that of other proteins

Structural analyses of several proteins have identified that conversion of non-proline peptide bonds from *trans* to *cis* conformations can be induced by external structural factors, such as metal binding, substrate binding or cofactor interaction that result in isomer-specific functional states.[8–11] In concanavalin A (ConA), binding of a metal ion in the binding site S2 is the driving force to initiate the *trans*-to-*cis* isomerization of the Ala207–Asp208 peptide bond, resulting a locked state of ConA. While metal ions are released from the binding site the *cis* peptide is destabilized and the structure tends to refold with a *trans* (Ala207–Asp208) peptide.[8] In hypoxanthine-guanine phosphoribosyltransferase (HGPRT) the Leu78–Lys79 peptide bond changes its geometric status during the course of catalysis, in which *cis/trans* isomerization of this peptide bond is related to the substrate binding (*trans* to *cis*) and product release (*cis* to *trans*), respectively.[9,10] The authors proposed that a portion of the energy released upon substrate binding to the apoenzyme is used to drive the Leu78–Lys79 peptide bond into the *cis* configuration, and that the energy released upon isomerization of the *cis* peptide bond back to the *trans* ground state helps to propel the substrate out of the active site.[10] The similar mechanism is reported in oxidation–reduction procedures of flavodoxin.[11] In these reports *cis/trans* conversion of non-proline peptide bond is governed by intermolecular binding events involving substrates, metal ions or cofactors. However, the present study revealed that the conversion of *cis* and *trans* isomeric states of a non-proline peptide bond in scorpion BmK toxins is governed by intramolecular structural factors as described above. A local unique structural motif (RT-CT) accounts for the tendency of the
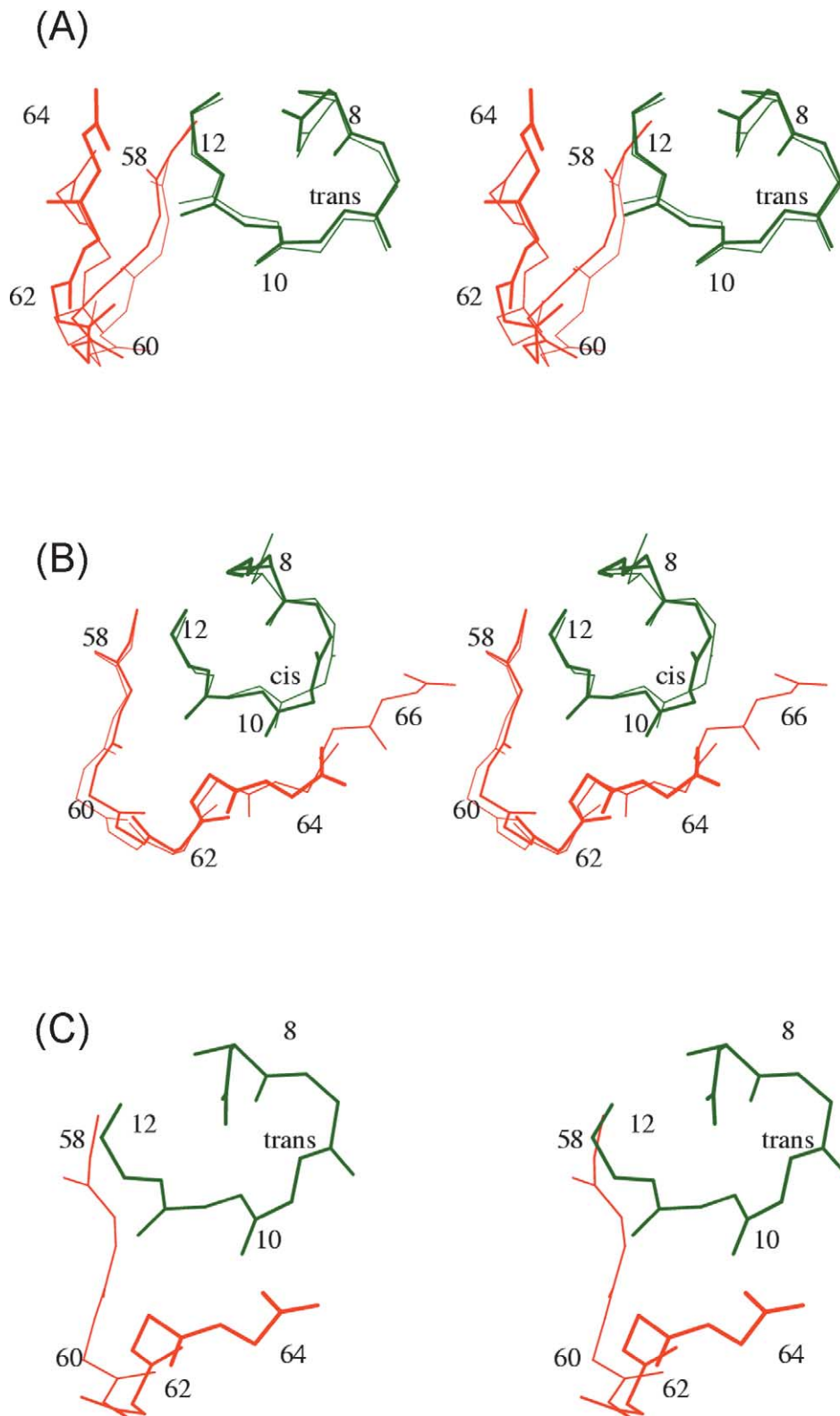
Figure 7. Three conformational states of site RT-CT formed by the five-residue reverse turn (in dark green) in association with C-terminal residues (in red) observed in scorpion α-toxins. (A) *trans*RT-*far*CT observed in BmK M8 (thick lines) and Aah2 (thin lines), in which the NH group of peptide bond 9–10 is situated inside the turn in compiling with the side-chain of the specific Asp8 and the C-terminal segment is far away from the peptide without any contact in between. (B) *cis*RT-*close*CT observed in BmK M1 (thick lines) and M7 (thin lines), in which both NH and CO groups of the *cis* peptide bond 9–10 are out of the reverse turn and the C-terminal segment is connect to the peptide *via* hydrogen bond N10–O64, in turn, close to the *cis* peptide bond 9–10. (C) *trans*RT-*close*CT observed in BmK M1 K8D mutant, in which the reverse turn adopts *trans*-containing organization but the orientation of the C-terminal residue is still close to the peptide bond 9–10 though there is no contact in between.

cis conformation, isomerization to the *trans* conformation and the co-existence of both isomers for the peptide bond 9–10. The *cis/trans* conversion is controlled by specific residues at position 8, which would result in the peptide 9–10 adopting a *trans*, *cis* or misfolded protein when it is replaced with Asp, Lys/Gln or Asn/Glu, respectively. All these properties found in BmK toxins showed a novel structural mechanism for *cis/trans* isomerization of a non-proline peptide bond, which is distinct from that observed in some other proteins, such as ConA, HGPRT and flevodoxin.

It was reported that many non-proline *cis* peptide bonds contain an aromatic residue and the presumed reason for this was the occurrence of an aliphatic–aromatic interaction from C–H to the Pi-system.[5] The aliphatic–aromatic interaction is an important factor for the stabilization of non-proline *cis* peptide bonds and may influence the *cis/trans* isomerization of these special peptide bonds. In principle, His10 of BmK M1 may accept such an interaction. However, careful examination of the contacts between residues 9 and 10 in BmK M1 and other *cis*-containing BmK toxins showed that there is no such an aliphatic–aromatic interaction as observed at non-proline *cis* peptide bonds in some other proteins. In fact, a homology toxin of BmK M1, BmK M4, in which residue 10 is Glu other than His, also showed a *cis* form of peptide bond 9–10.[20] It seems that the stabilization of the *cis* form in BmK toxins is not dependent on the close aliphatic–aromatic contacts, but the tertiary interaction between the *cis* peptide bond and the C-terminal segment.

A series of experimental data suggest that the *cis/trans* isomerization found in BmK toxins is pH-independent. Actually the crystal structures of BmK M1, M2, M4 and mutant (K8Q) obtained in a wide range of pH values (from pH 4.6–8.5) can present the same *cis* form of peptide bond 9–10. The toxins with either His (BmK M1) or Glu (BmK M4) at position 10 can adopt the *cis* peptide bond, which seems not relevant to the protonating status of His10. The mutant K8D crystallized in a range of pH 5–8 can present the same conformation as *trans*. Besides, it is definitely known that the co-existence of *cis* and *trans* conformations is due to the abrogation of the interaction between the peptide bond 9–10 and C terminus, but not related to the side-chain interactions. All these data indicate that the *cis/trans* isomerization observed in BmK toxins is pH-independent. Actually the distinct isomeric states of the peptide bond 9–10 in BmK toxins are mainly governed by the specific intramolecular interactions and the molecular switch at position 8 is sequence-dependent rather than pH-dependent.

Experimental Procedures

Protein production

BmK M7 was purified from BmK venom by gel-filtration and ion-exchange chromatography as described.[29] The molecular mass, isoelectric point and toxicity of isolated BmK M7 were confirmed prior to crystallization. Five mutants of BmK M1 (Lys8Asp (K8D), Lys8Asn (K8N), Lys8Glu (K8E), Lys8Gln (K8Q) and Pro9Ser (P9S)) were produced by one-step PCR using synthetic primers: primer1 (5′-CGTCTAGATAAAA GAAATTCTGTTCGGGATGCTTATATTGCC**GAT**C CC CATAAC-3′ (K8D), 5′-CGTCTAGATAAAAGAAATTC TGTTCGGGATGCTTATA TTGCC**AAT**CCCCATAAC-3′ (K8N), 5′-CGTCTAGATAAAAGAAATTCTGTTCGGG ATGCTTATAT̲TGCC**GAA**CCCCATAAC-3′ (K8E), 5′-CGTCTAGATAAAAGAAATT CTGTTCGGGATGCTTA TATTGCC**CAA**CCCCATAAC-3′ (K8Q), 5′-CGTCTA̲ GATA̲ AAAGAAATTCTGTTCGGGATGCTTATATTGC CAAG**AGT**CATAACTGT-3′ (P9S)) including KEX2 protease linker and XbaI restriction site and primer2 (5′-CGAAGCTTTTAATGGCA TTTTCCTGGTAC-3′ (same for all five mutants)) with HindIII site and the pVT 102U/α-wild-type BmK M1 yeast expression vector, followed by expression in *Saccharomyces cerevisiae* S-78 as described.[30] BmK M1 mutants were purified by two successive chromatographic steps. First, cationic-exchange chromatography was carried out on a CM32-cellulose column. Eluted fraction containing the target protein was then purified by reverse phase chromatography using a Sephasil® peptide C18 column on an AKTA Purifier chromatography system (Pharmacia Biotech, Sweden). Details of the purification procedure are similar to that described elsewhere.[23] The final purified samples were examined by ESI mass spectrometry using an API 3000 triple quadrupole mass spectrometer (Perkin-Elmer Sciex Instruments, Canada).

Biossay of BmK M1 mutants

Using 0.9% (w/v) NaCl as a negative control and rBmK M1 as a positive control, the toxicity of the mutants was determined in mice (male, specified pathogen-free level, 18–20 g of body weight). Each group consisted of ten mice. Various doses of toxin mutants were dissolved in 0.9% NaCl and injected into the mice through the tail vein. Survival times (times between injection and death), reaction, and doses were recorded. Evaluation of toxicity was based on the determination of LD_{50} (the dose capable of statistically killing 50% of the mice) as defined in the method described by Meier & Theakston.[24]

Crystallization and data collection

BmK M7 was crystallized at room temperature by the hanging-drop vapor-diffusion method using equal volumes of BmK M7 (10 mg/ml) and 0.65 M ammonium sulfate, 100 mM Tris–HCl (pH 8.5) using 1% (v/v) ethanol as an additive. The largest crystals grew to 0.5 mm× 0.2 mm×0.2 mm within one month. The K8D, K8Q and P9S mutants of BmK M1 were crystallized similarly to BmK M7, with the exception of the crystallization buffer additives used. These were 1.5 M sodium phosphates at pH 6.0 for K8D, 3.2 M sodium phosphate at pH 4.6 and 5% (v/v) PEG400 as an additive for P9S and 30% (v/v) PEG8000 and 0.1 M sodium cacodylate at pH 6.5 with 0.2 M ammonium sulfate as an additive for K8Q.

Diffraction data of BmK M7 and the K8D and P9S BmK M1 mutants were collected at room temperature using synchrotron radiation ($\lambda = 1.0$ Å) on an ADSC Quantum 4 CCD detector at the beam line BL18B of the Photon Factory in Tsukuba, Japan. For BmK M7, the crystal could diffract to at least 1.4 Å. Diffraction data of mutant K8Q

were collected on a Mar345 image-plate detector using CuK$_\alpha$ radiation ($\lambda = 1.5418$ Å). The diffraction data were processed and analyzed by using DPS/MOSFLM/CCP4[31–33] and the HKL suite of programs.[34] The results showed that there are two monomers in the asymmetric unit of BmK M7, but only one in those of each of the three BmK M1 mutants. The crystal parameters and data collection statistics are listed in Table 3.

Structure determination and refinement

The structures of BmK M7 and three mutants of BmK M1 were solved by molecular replacement using the program AMoRe.[35] For BmK M7, a homologous model of BmK M8 with PDB code 1snb[19] was used as a model. With data from 8 Å to 3 Å, in the first run of AMoRe, one solution was found with correlation coefficient (cc) of 0.34 and R factor of 0.50, indicating a potential location of the first molecule in the asymmetric unit. Fixing the position of this first molecule and extending the molecular replacement search for a second unique solution resulted in improved cc and R factor values 0.57 and 0.42, respectively, after rigid-body refinement. The structures of the three mutants of BmK M1 were also solved by molecular replacement using the structure of the native BmK M1 (PDB code 1sn1) as a model. The unique solutions for the rotation and translation searches were obvious, exhibiting initial cc and R factor values of about 0.60 and 0.40, respectively, after rigid body refinement.

The initial structures of BmK M7 and the three mutants of BmK M1 were refined with CNS[36] and the models were rebuilt with TURBO-FRODO[44] and O,[37] with 10% of the data retained for cross-validation purposes. For BmK M7, no non-crystallographic symmetry restriction was applied during the refinement. Iterative rounds of model building and minimization lowered the R_{cryst} to 0.253 and R_{free} to 0.280. After individual B factor refinement and adding water molecules, the R_{cryst} was 0.1679 and R_{free} was 0.1864. When applying the *cis* and *trans* dual configurations to the 9–10 peptide bond in molecule B, the R_{cryst} and R_{free} were reduced to 0.1669 and 0.1840, respectively. Finally, anisotropic B factor refinement using REFMAC5[38] lowered the R_{cryst} and R_{free} values to 0.142 and 0.164, respectively. Structural refinements of the three BmK M1 mutant structures were performed using iterative rounds of positional and individual B factor refinement, as well as the addition of solvent molecules resulting in a final refinement of the K8D, K8Q and P9S BmK M1 mutant structures at resolutions of 1.50 Å, 1.85 Å and 1.40 Å resulted in R_{cryst} values of 0.165, 0.171 and 0.192 and corresponding R_{free} values of 0.183, 0.197 and 0.216, respectively (Table 3).

Protein Data Bank accession code

The coordinates and structure factors of BmK M7 and the three mutants of BmK M1 (K8D, K8Q and P9S) have been deposited to the RCSB PDB with accession numbers 1KV0, 1T7A, 1T7B and 1T7E, respectively.

Table 3. X-ray data collection and refinement statistics of BmK M7 and three mutants of BmK M1

Species	BmK M7	K8D	K8Q	P9S
Unit cell				
a (Å^2)	32.76	47.45	47.59	46.91
b (Å^2)	32.76	44.34	44.06	46.91
c (Å^2)	176.82	25.49	25.51	53.75
α, β, γ (deg.)	90, 90, 120	90, 90, 90	90, 90, 90	90, 90, 120
Space group	$P3_121$	$P2_12_12$	$P2_12_12$	$P3_221$
Resolution range (Å)				
Overall	29.3–1.40	30.0–1.50	30.0–1.85	30.0–1.40
Highest resolution shell	1.48–1.40	1.55–1.50	1.92–1.85	1.48–1.40
Number of observations	57,131	41,017	28,173	97,281
Number of unique reflections	19,260	8946	4831	13,889
Completeness[a] (%)	85.8 (74.6)	98.1 (93.3)	97.6 (93.8)	100.0 (100.0)
R_{merge}[a] (%)	4.0 (20.1)	5.2 (17.5)	8.3 (28.3)	5.3 (35.5)
$I/\sigma(I)$[a]	10.0 (3.6)	28.3 (8.7)	22.0 (6.0)	7.9 (2.0)
B factor from Wilson plot (Å^2)	13.0	17.5	19.8	20.4
R_{cryst}[b]	0.142	0.165	0.171	0.192
R_{free}[b] (10% data)	0.164	0.183	0.197	0.216
R.m.s. deviations				
Bond length (Å)	0.017	0.004	0.008	0.013
Bond angles (deg.)	1.983	1.300	1.550	1.670
Chiral (deg.)	0.152			
Ramachandran plot				
Core region (%)	91.3	92.6	90.7	87.3
Additional allowed region (%)	8.7	7.4	9.3	12.7
Protein model				
Protein non-H atoms	1008	516	517	520
Number of phosphate groups	–	–	–	3
Water molecules	118	84	50	51
Average temperature factors (Å^2)				
Protein	14.5, 19.1	10.4	17.5	16.6
Phosphate groups	–	–	–	22.0
Water molecules	31.4	27.5	30.3	32.3

[a] Values in parentheses refer to the outer resolution shell.
[b] $R_{cryst} = \sum ||F_o| - |F_c||/\sum |F_o|$, where F_c is the calculated structure factors. R_{free} is as for R_{cryst} but calculated for a randomly selected 10% of reflections not included in the refinement.

Acknowledgements

References

1. Ramachandran, G. N. & Sasisekharan, V. (1968). Conformation of polypeptides and proteins. *Advan. Protein Chem.* **23**, 283–438.

2. Ramachandran, G. N. & Mitra, A. K. (1976). An explanation for the rare occurrence of *cis* peptide units in proteins and polypeptides. *J. Mol. Biol.* **107**, 85–92.

3. Stewart, D. E., Sarkar, A. & Wampler, J. E. (1990). Occurrence and role of *cis* peptide bonds in protein structures. *J. Mol. Biol.* **214**, 253–260.

4. Weiss, M. S., Jabs, A. & Hilgenfeld, R. (1998). Peptide bonds revisited. *Nature Struct. Biol.* **5**, 676.

5. Jabs, A., Weiss, M. S. & Hilgenfeld, R. (1999). Non-proline *cis* peptide bonds in proteins. *J. Mol. Biol.* **286**, 291–304.

6. Pal, D. & Chakrabarti, P. (1999). *Cis* peptide bonds in proteins: residues involved, their conformations, interactions and locations. *J. Mol. Biol.* **294**, 271–288.

7. Pappenberger, G., Aygun, H., Engels, J. W., Reimer, U., Fischer, G. & Kiefhaber, T. (2001). Nonprolyl *cis* peptide bonds in unfolded proteins cause complex folding kinetics. *Nature Struct. Biol.* **8**, 452–458.

8. Bouckaert, J., Dewallef, Y., Poortmans, F., Wyns, L. & Loris, R. (2000). The structural features of concanavalin A governing non-proline peptide isomerization. *J. Biol. Chem.* **275**, 19778–19787.

9. Heroux, A., White, E. L., Ross, L. J. & Borhani, D. W. (1999). Crystal structures of the *Toxoplasma gondii* hypoxanthine-guanine phosphoribosyltransferase-GMP and -IMP complexes: comparison of purine binding interactions with the XMP complex. *Biochemistry*, **38**, 14485–14494.

10. Heroux, A., White, E. L., Ross, L. J., Davis, R. L. & Borhani, D. W. (1999). Crystal structure of *Toxoplasma gondii* hypoxanthine-guanine phosphoribosyltransferase with XMP, pyrophosphate, and two Mg(2+) ions bound: insights into the catalytic mechanism. *Biochemistry*, **38**, 14495–14506.

11. Ludwig, M. L., Pattridge, K. A., Metzger, A. L., Dixon, M. M., Eren, M., Feng, Y. & Swenson, R. P. (1997). Control of oxidation-reduction potentials in flavo-doxin from *Clostridium beijerinckii*: the role of confor-mation changes. *Biochemistry*, **36**, 1259–1280.

12. Bates, P. A., Dokurno, P., Freemont, P. S. & Sternberg, M. J. (1998). Conformational analysis of the first observed non-proline *cis*-peptide bond occurring within the complementarily determining region (CDR) of an antibody. *J. Mol. Biol.* **284**, 549–555.

13. Odefey, C., Mayr, L. M. & Schmid, F. X. (1995). Non-prolyl *cis–trans* peptide bond isomerization as a rate-determining step in protein unfolding and refolding. *J. Mol. Biol.* **245**, 69–78.

14. Vanhove, M., Raquet, X., Palzkill, T., Pain, R. H. & Frere, J. M. (1996). The rate-limiting step in the folding of the *cis*-Pro167Thr mutant of TEM-1 beta-lactamase is the *trans* to *cis* isomerization of a non-proline pep-tide bond. *Proteins: Struct. Funct. Genet.* **25**, 104–111.

15. Wheeler, K. A., Hawkins, A. R., Pain, R. & Virden, R. (1998). The slow step of folding of *Staphylococcus aureus* PC1 beta-lactamase involves the collapse of a surface loop rate limited by the trans to *cis* isomeriza-tion of a non-proline peptide bond. *Proteins: Struct. Funct. Genet.* **33**, 550–557.

16. Catterall, W. A. (1979). Binding of scorpion toxin to receptor site associated with sodium channels in for muscle. *J. Gen. Physiol.* **74**, 357–391.

17. Rochat, H., Berhard, P. & Couraud, F. (1979). Scorpion toxin chemistry and mode of action. In *Advances in Cylopharmacologyl* (Cecarelli, B. & Chementi, F., eds), vol. 3, pp. 325–334, Raven Press, New York.

18. Gordon, D., Martin-Eauclaire, M. F., Cestele, S., Kopeyan, C., Carlier, E. Khalifa, R. B. *et al*. (1996). Scorpion toxins affecting sodium current inactivation bind to distinct homologous receptor sites on rat brain and insect sodium channels. *J. Biol. Chem.* **271**, 8034–8045.

19. Li, H. M., Wang, D. C., Zeng, Z. H., Jin, L. & Hu, R. Q. (1996). Crystal structure of an acidic neurotoxin from scorpion *Buthus martensii* Karsch at 1.85 Å resolution. *J. Mol. Biol.* **261**, 415–431.

20. He, X. L., Li, H. M., Zeng, Z. H., Liu, X. Q., Wang, M. & Wang, D. C. (1999). Crystal structures of two alpha-like scorpion toxins: non-proline *cis* peptide bonds and implications for new binding site selectivity on the sodium channel. *J. Mol. Biol.* **292**, 125–135.

21. Housset, D., Habersetzer-Rochat, C., Astier, J. P. & Fontecilla-Camps, J. C. (1994). Crystal structure of toxin II from the scorpion *Androctonus australis* Hector refined at 1.3 Å resolution. *J. Mol. Biol.* **238**, 88–103.

22. Lawrence, M. C. & Colman, P. M. (1993). Shape complementarily at protein/protein interfaces. *J. Mol. Biol.* **234**, 946–950.

23. Sun, Y. M., Bosmans, F., Zhu, R. H., Goudet, C., Xiong, Y. M., Tytgat, J. & Wang, D. C. (2003). Importance of the conserved aromatic residues in the scorpion alpha-like toxin BmK M1: the hydrophobic surface region revisited. *J. Biol. Chem.* **278**, 24125–24131.

24. Meier, J. & Theakston, R. D. G. (1986). Approximate LD$_{50}$ determination of snake venoms using eight to ten animals. *Toxicon*, **24**, 395–401.

25. Hutchinson, E. G. & Thorton, J. M. (1994). A revised set of potentials for β-turn formation in proteins. *Protein Sci.* **3**, 2207–2216.

26. Rogers, J. C., Qu, Y., Tanada, T. N., Sheuer, T. & Catterall, W. A. (1996). Molecular determinants of high affinity binding of α-scorpion toxin and sea anemone toxin in the S3-S4 extracellular loop in domain IV of the sodium channel α subunit. *J. Biol. Chem.* **271**, 15950–15959.

27. Gordon, D., Sevarin, P., Gurevitz, M. & Zinn-Justin, S. (1998). Functional anatomy of scorpion toxins, affect-ing sodium channels. *Toxicol. Toxin Rev.* **17**, 131–159.

28. Wang, C. G., Gilles, N., Hamon, A., Le Gall, F., Stankiewicz, M. Pelhate, M. *et al*. (2003). Exploration of the functional site of a scorpion α-like toxin by site-directed mutagenesis. *Biochemistry*, **42**, 4699–4708.

29. Guan, R. J., He, X. L., Wang, M., Ye, X., Li, G. P. & Wang, D. C. (2002). Purification and crystallization of a new alpha-like toxin with cardiac toxicity from scorpion *Buthus martensii* Karsch. *Protein Pept. Letters*, **9**, 441–449.

30. Shao, F., Xiong, Y. M., Zhu, R. H., Ling, M. H., Chi, C. W. & Wang, D. C. (1999). Expression and purification of the BmK M1 neurotoxin from the scorpion *Buthus martensii* Karsch. *Protein Expr. Purif.* **17**, 358–365.

31. Nielsen, C., Arvai, A., Szebenyi, D. M. E., Deacon, A.,

Thiel, D. J., Bolotovsky, R., Van Zandt, K. C. & Rossmann, M. (1998). DPS: a data processing system for oscillation method data from a 2×2 mosaic CCD detector. Abstract 11.06.06, ACA Meeting July 18–23.

32. Leslie, A. G. W. (1990). *Crystallographic Computing*: Oxford University Press.

33. Collaborative Computational Project Number 4. (1994). The CCP4 suite: programs for protein crystallography. *Acta Crystallog. sect. D*, **50**, 760–763.

34. Otwinowski, Z. & Minor, W. (1997). Processing of X-ray diffraction data collected in oscillation mode. *Methods Enzymol.* **276**, 307–326.

35. Navaza, J. (1994). AMoRe—an automated package for molecular replacement. *Acta Crystallog. sect. A*, **50**, 157–163.

36. Brünger, A. T., Adams, P. D., Clore, G. M., DeLano, W. L., Gros, P. Grosse-Kunstleve, R. W. *et al*. (1998). Crystallography & NMR system: a new software suite for macromolecular structure determination. *Acta Crystallog. sect. D*, **54**, 905–921.

37. Jones, T. A., Zou, J. Y., Cowan, S. W. & Kjeldgaard, M. (1991). Improved methods for binding protein models in electron density maps and the location of errors in these models. *Acta Crystallog. sect. A*, **47**, 110–119.

38. Murshudov, G. N., Vagin, A. A. & Dodson, E. J. (1997). Refinement of macromolecular structures by the maximum-likelihood method. *Acta Crystallog. sect. D*, **53**, 240–255.

39. Possani, L. D., Becerril, B., Delepierre, M. & Tytgat, J. (1999). Scorpion toxins specific for Na+-channels. *Eur. J. Biochem.* **264**, 287–300.

40. Thompson, J. D., Higgins, D. G. & Gibson, T. J. (1994). CLUSTAL W: improving the sensitivity of progressive multiple sequence alignment through sequence weighting, position-specific gap penalties and weight matrix choice. *Nucl. Acids Res.* **22**, 4673–4680.

41. Barton, G. J. (1993). ALSCRIPT: a tool to format multiple sequence alignments. *Protein Eng.* **6**, 37–40.

42. Kraulis, P. J. (1991). MOLSCRIPT: a program to produce both detailed and schematic plots for protein structures. *J. Appl. Crystallog.* **24**, 946–950.

43. Merritt, E. & Murphy, M. E. P. (1994). Raster3D version 2.0: a program for potorealistic molecular graphics. *Acta Crystallog. sect. D*, **50**, 869–873.

44. Roussel, A. & Cambillau, C. (1992). *TURBO-FRODO*. Marseille, France: Biographics, LCCMB.